Desalination and Water Treatment
www.deswater.com

doi: 10.5004/dwt.2023.29218

283 (2023) 130–140
January

Enhanced adsorption of fluoride ion by polyethylenimine modified diatomite in aqueous solution: adsorption optimization, models, and mechanism

Yanzhuo Zhang[a,b,*], Haiqin Zhang[a], Jing Zhao[b], Xiaozhuan Zhang[a]

[a]*Water Resource Protection and Utilization in Coal Mining, Beijing 100011, China, emails: zhangadsorption@126.com (Y. Zhang), 20039431@ceic.com (H. Zhang), zhangxiaozhuan0103@126.com (X. Zhang)*
[b]*School of Environment, Henan Normal University, Key Laboratory for Yellow River and Huai River Water Environmental and Pollution Control, Ministry of Education, Henan Key Laboratory for Environmental Pollution Control, International Joint Laboratory on Key Techniques in Water Treatment, Xinxiang, Henan 453007, China, email: zjjb19980315@163.com (J. Zhao)*

Received 17 August 2022; Accepted 11 December 2022

ABSTRACT

There is a growing problem of excessive fluoride ion (F^-) in mine water in western China and it is urgent to identify appropriate treatment strategies. In this work, we tested polyethylenimine-modified diatomite for adsorption of low concentration F^- from aqueous solution. Fourier-transform infrared spectroscopy analysis suggested amino group ($–NH_2$) may be the main functional group promoting adsorption. Scanning electron microscopy and Brunauer–Emmett–Teller–Barrett–Joyner–Halenda analysis showed that the modified diatomite surface became smooth and the specific surface area decreased slightly with modification. The optimal pH, temperature, and dosage of polyethylenimine modified diatomite (PEI/DT) were determined as 2.0°C, 5°C, and 0.2 g/L, respectively. The whole adsorption process can be completed in 20–30 min. The adsorption data were better fit to the Langmuir model (average R^2 = 0.9962) to describe the adsorption process than the Freundlich model (average R^2 = 0.9413). The adsorption efficiency of F^- by PEI/DT was highest at 5°C, with a maximum saturated adsorption capacity (q_{max}) of 28.62 mg/g. The pseudo-second-order kinetic model (average R^2 = 0.9992) is more suitable to describe the overall adsorption process and the pseudo-first-order kinetic model (average R^2 = 0.7318) can only describe the initial stage of adsorption. Thermodynamic parameters confirm that the adsorption process is a spontaneous exothermic process. Overall, the results show that the prepared PEI/DT can potentially be used as an adsorbent to remove F^- from mine water.

Keywords: Polyethylenimine; Modified diatomite; Fluoride ion; Adsorption; Optimization

1. Introduction

In recent years, coal mining has gradually shifted from the Middle East to the west part of China [1]. To address mine drainage loss and protect water resources, the National Energy Group built a number of underground reservoirs [2]. Although this addressed the loss of water resources, there have been some problems with water quality, including a concentration of fluoride ion (F^-) that exceeds the safety standard [3]. People routinely drinking groundwater with excessive fluoride ion will experience dental and bone fluorosis [4]. Therefore, excessive F^- in water poses a huge potential threat to local residents as well as the local water environment [5]. Therefore, there is an urgent need to address the problem of excessive F^- in water.

Many methods have been developed for the treatment of fluorine-containing wastewater, with precipitation and adsorption the most commonly used methods [6–8].

* Corresponding author.

Calcium salt precipitation method is generally used for industrial wastewater with a high concentration of F^- [9]. Lime cream can be added to promote generation by F^- and Ca of CaF_2 precipitation. Lacson et al. [10] used recovered calcium carbonate to remove 98% of F from an aqueous solution containing a high concentration of F^- (4,000 mg/L) at a pH of 2–6. Wang et al. [11] used biosynthetic crystals separated by calcium carbonate precipitation to remove F^- (1,500–3,500 mg/L) from groundwater, with a maximum saturated adsorption capacity of 5.10 mg/g and a removal rate of 98.24%. However, the concentration of F^- in underground reservoirs is typically much lower, about 5 mg/L, and precipitation methods are not suitable for treatment of this low F^- concentration.

Adsorption technology is simple, easy to operate, and typically is relatively low in cost. Adsorption is considered the most effective method to remove low concentrations of F^- (1–5 mg/L). Dehghani et al. [12] used chitosan-Fe_3O_4 to adsorb fluorine ions, with a maximum saturation adsorption capacity of 2.30 mg/g. Cheng et al. [13] used activated alumina to adsorb fluorine ions under neutral conditions, with q_{max} of 2.74 mg/g. Al–Ce hybrid was used for adsorption of F^- with a maximum saturated adsorption capacity at 180 min of 27.5 mg/g. Despite these promising results, large-scale application of these methods has been limited because some adsorbents have limited adsorption capacity or too much adsorption time is required [14]. Effective adsorption technology requires the careful selection of a suitable adsorbent and an effective modification method. The main component of diatomite is SiO_2, which has good mechanical properties and stable performance in acidic and alkaline solution [15]. Diatomite was previously modified as an adsorbent carrier for efficient adsorption of cationic pollutants [16]. However, F^- is a typical anionic pollutant in water, so for the removal of F^-, different reagents must be selected for modification of diatomite.

Polyethylenimine (PEI) is a water–soluble polymer with high adhesion and absorbability and can be loaded on the surface of diatomite carrier. After dissolving PEI in water, amino groups ($–NH_2$) can be protonated and form cationic amino groups (NH_3^+) with H^+ in aqueous solution [17]. Protonated NH_3^+ binds to negatively charged diatomite in aqueous solution, confirming the successful loading of PEI to give a positively charged surface of modified diatomite. PEI was loaded on the adsorbent surface and used to adsorb a variety of anionic dyes [18]. Through electrostatic attraction, the NH_3^+ groups on the surface of PEI can efficiently adsorb dyes from water, with the dyes completely adsorbed on the adsorbent surface [19,20]. Although there have been no reports of high adsorption efficiency for F^- at low concentration (1–5 mg/L), few studies have tested polyethylenimine-modified diatomite for this purpose.

In this work, polyethylenimine-modified diatomite (PEI/DT) was used to adsorb fluorine ions in aqueous solution. Diatomite and modified diatomite were characterized by scanning electron microscopy (SEM), Brunauer–Emmett–Teller–Barrett–Joyner–Halenda (BET–BJH), X-ray diffraction (XRD), and adsorption experiments. The optimum parameters of F^- adsorption in aqueous solution were determined by varying temperature, dosage, and contact time. The isothermal adsorption and adsorption kinetics models were used to describe the adsorption data and determine the thermodynamic parameters of adsorption states, such as enthalpy ($\Delta H°$), entropy ($\Delta S°$), and Gibbs function values ($\Delta G°$).

2. Materials and methods

2.1. Pretreatment process of diatomite

Diatomite was obtained from a power plant in Burian and the specific ingredients are listed in Table S1. The sample was washed several times with distilled water and HCl (0.5 m) to remove impurities and organic matter, dried at 105°C, and sealed and stored before subsequent use. The modified diatomite was prepared by surface loading of high molecular organic polymer. For modification, 1,000 mL distilled water and 10 mL polyethylenimine colloid solution were mixed and stirred until the polyethylenimine completely dissolved, becoming a light-yellow viscous solution.

2.2. Reagents

NaF (98%), NaOH (96%), and polyethylenimine (MW = 1,800, 99%) were purchased from Shanghai Aladdin Co., Ltd., China. HCl (35%) was purchased from Tianjin Damao Chemical Reagent Company, China. Deionized water (18 MΩ/cm) was used for all experiments.

2.3. Batch adsorption experiment

The 100 mg/L F^- stock solution was prepared by weighing 225.56 g NaF. A certain volume of the stock solution was transferred into a conical flask with a volume of 100 mL for adsorption experiments. A certain amount of modified diatomite was thoroughly mixed with F^- solution. The mixed solution was stirred at 180 rpm in a thermostatic oscillator until reaching adsorption equilibrium. The concentration of F^- was measured at certain time intervals, and removed samples were centrifuged at 3,200 rpm for 2 min before measurement of the concentration with a F^- meter (Leici, PXSJ-216F, China). For batch adsorption, the pH was adjusted by addition of 0.5 M HCl or 0.5 M NaOH.

Different parameters in the adsorption process (pH, dosage, and contact time) were varied to determine the optimum conditions for F^- adsorption. The solution pH was adjusted to 2, 3, 4, 5, 6, and 7, at temperature, initial concentration, and dosage of 25°C, 5 mg/L, and 0.2 g/L, respectively. Similarly, different dosages (0.1, 0.2, 0.3, 0.4 and 0.5 g/L), different contact times (1, 3, 5, 10, 15, 20, 30, 50, and 70 min) and different temperatures (5°C, 10°C, and 15°C) were analyzed as factors affecting the adsorption process [21,22]. For the adsorption experiments, 100 mL F^- solution was mixed with adsorbent and adsorption was allowed for 30 min before the measurement of residual F^- concentration.

After reaching the adsorption equilibrium, the equilibrium adsorption capacity (q_e) and F^- removal efficiency (R) of PEI/FA were calculated according to the following equations [23]:

$$q_e = \frac{V\left(C_0 - C_e\right)}{M} \tag{1}$$

$$R = \frac{C_0 - C_e}{C_0} \times 100 \quad (2)$$

where q_e is the equilibrium adsorption capacity of adsorbent, mg/g; C_0 is the initial concentration of F^-, mg/L; C_e is the equilibrium adsorption concentration, mg/L; V is the volume of the aqueous solution, L; M is the mass of the adsorbent, g.

2.4. Instrument and equipment

Fourier-transform infrared spectroscopy (Thermo Fisher Scientific, FTIR, Nicolet iS10, USA) was used to detect functional groups and chemical bonds on the surface of adsorbents. The pH in the solution was adjusted by addition of HCl and measurement with a pH meter (WTW, MIQ/TC 2020, Germany). The specific surface area and pore-size of adsorbents were analyzed by BET–BJH (Micromeritics Instrument Corp., ASAP 2020, USA). The composition and crystal type of the adsorbent were analyzed by X-ray diffractometer (Shimadzu Corporation, XRD 6100, Japan). The morphology and surface structure of the adsorbent were analyzed by scanning electron microscopy (SEM, Hitachi S-4800, Japan). The thermal stability of the adsorbent was measured using a thermogravimetric analyzer (TGA, NETZSCH STA 449 C, Germany).

3. Results and discussion

3.1. Characterization of diatomite

The surface morphology and structure of diatomite were observed by SEM before and after modification (Fig. 1). Fig. 1a shows that the unmodified diatomite after pretreatment exhibits a rough surface and many mesh-shaped pores, ideal characteristics of an adsorbent [24]. Fig. 1b shows that the surface porosity of diatomite decreased after modification, indicating the successful loading of PEI onto the surface of diatomite. Although the modification decreased the surface porosity, it can significantly increase the adsorption efficiency of F^-.

The composition of diatomite and modified diatomite was qualitatively analyzed by XRD. As shown in Fig. 1c, the diatomite used here was mainly composed of SiO_2, with smaller amounts of cristobalite, quartz, and montmorillonite. This composition of modified diatomite is consistent with that of diatomite earth (Fig. 1d). XRD confirmed SiO_2 as the main component in diatomite.

The specific surface area and pore size were measured to directly evaluate the adsorption capacity of F^-. As shown in Table S2, the specific surface areas of diatomite and PEI/DT were 65.86 and 47.07 m^2/g, indicating the loading of PEI on the surface of modified diatomite. Loading can lead to the blockage of surface pores, thus reducing the specific surface area [25]. The change of total porosity is positively correlated with the change of specific surface area. However, the average pore size is negatively correlated with the specific surface area and the average pore size decreases with the increase of specific surface area. The average pore sizes of were measured for diatomite and PEI/DT as 3.38 and 4.89 nm, respectively. As depicted in Fig. S1, the original diatomite has the largest number of pores with the size of 9.2 nm, while the modified diatomite has the largest number of pores 44.7 nm in size. This suggests that the modification of PEI may block the pores of diatomite, thus reducing the number of small pores. Although many pores are blocked, the modified reagent can greatly improve the adsorption capacity of the adsorbent for improved F^- adsorption efficiency.

FTIR can reveal the composition of functional groups and chemical bonds on the surface of the adsorbent. The presence of new functional groups was confirmed by comparing the patterns for diatomite before and after modification. Fig. 1e shows that the peaks of the main functional groups in the diatomite mainly occur at 3,439; 1,640; 1,467 and 1,081 cm^{-1}. The peak at 3,439 cm^{-1} may be hydrogen atom in Si–H bond, 1,640 cm^{-1} may correspond to bending vibration of H–OH bond, the peak of 1,467 cm^{-1} may be caused by C–O stretching vibration and bending vibration of H–OH, and the peak value at 1,081 cm^{-1} may represent Si–O–H bond. After modification, the peaks mainly occurred at 3,445; 2,347; 2,453; 1,646; 1,469 and 1,093 cm^{-1}, with strong peaks at 2,347 and 2,453 cm^{-1} likely corresponding to amino group ($–NH_2$), an important functional group for the adsorption of F^- on PEI/DT. Compared with the pristine diatomite, the new peaks of 2,347 and 2,453 cm^{-1} indicated successful loading of the polyethylenimine onto the surface of diatomite [26].

TGA is an index that can be used to evaluate the thermal stability of diatomite and explain the proportion of mass loss of diatomite before and after modification with increased temperature [27]. Fig. 1f shows that the mass fractions of diatomite and modified diatomite decreased with the increase of temperature. Increasing temperature from 0°C–200°C, the weights of diatomite and modified diatomite decreased rapidly because the weight loss in this temperature range is due to changes in the moisture content in the adsorbent. At temperatures above 200°C, the change trend of the weight of the adsorbent slows, mainly corresponding to the loss of water and the volatilization of impurities. The SiO_2 in diatomite is resistant to high temperatures, with a melting point of more than 1,700°C. When the temperature reached 700°C, the weight of the adsorbent basically remained unchanged, indicating that the modified diatomite exhibits high thermal stability.

3.2. Optimization of adsorption parameters

3.2.1. Effect of pH on F^- adsorption

The process parameters were varied to optimize adsorption. The pH value of the solution has a significant influence on the surface charge of PEI/DT and the adsorption capacity of F^- in the solution [28]. Consistently, pH greatly affected the adsorption efficiency of F^- by PEI/DT in aqueous solution. Fig. 2 shows the change of F^- adsorption efficiency under different pH. At pH = 2, the removal efficiency of F^- reached the maximum of 97.56%. In the pH range from 2 to 7, the adsorption efficiency of F^- decreased obviously, reaching the lowest adsorption efficiency (60.24%) at pH = 7. Electrostatic attraction is an important principle of adsorption. The effect of pH on adsorption is mainly

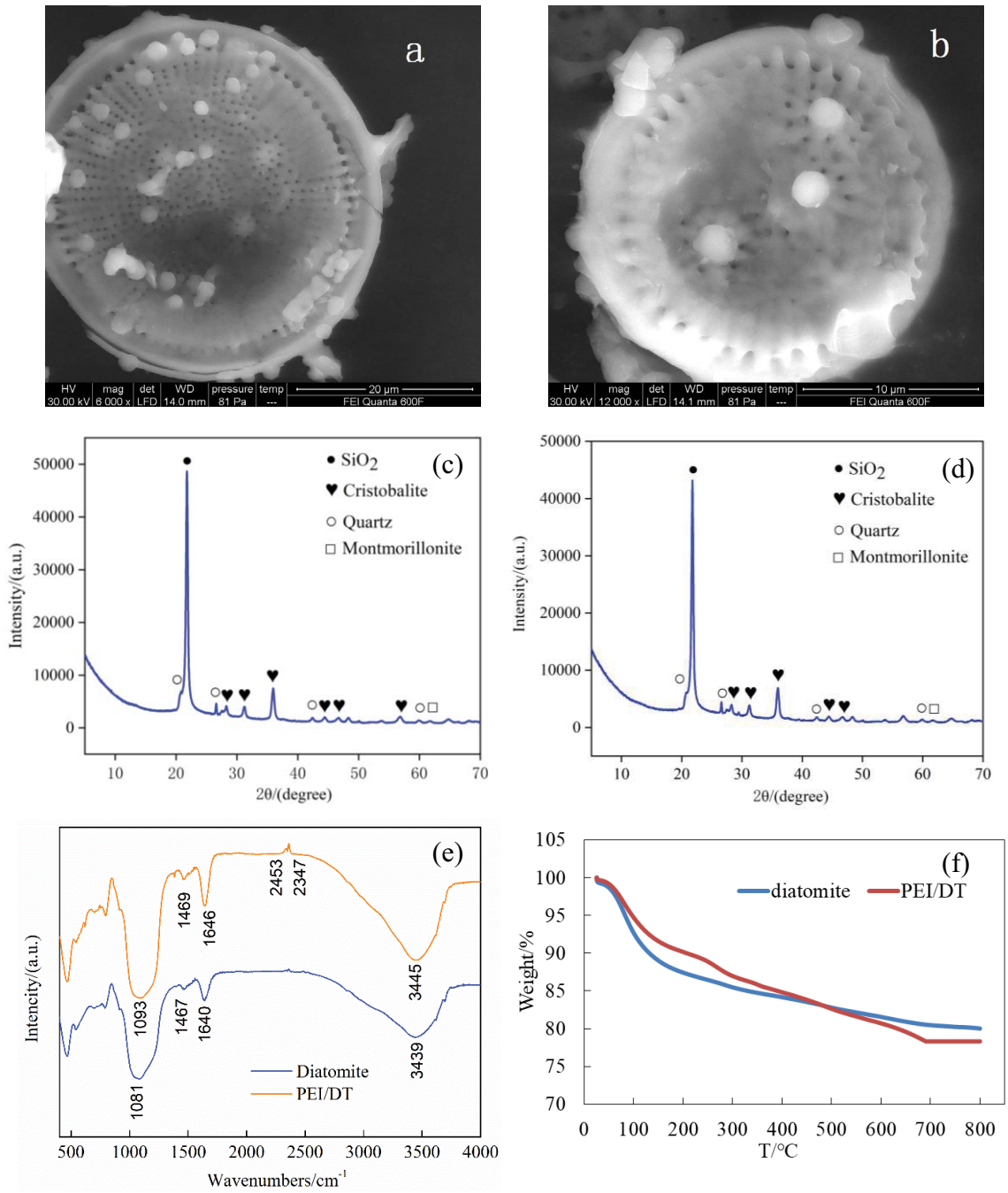

Fig. 1. Physico-chemical characterization of diatomite and modified diatomite.

related to the isoelectric point of diatomite in water, and the isoelectric point of PEI/DT is 2.2.

During the adsorption process, the presence of H^+ ions protonate $–NH_2$ on the surface of PEI/DT into NH_3^+ [Eq. (3)].

$$\frac{PEI}{DT}-NH_2+H^+ \rightleftarrows \frac{PEI}{DT}-NH_3^+ \quad (3)$$

$$\frac{PEI}{DT}-NH_3^+ + F^- \rightleftarrows \frac{PEI}{DT}-NH_3^+ - F^- \quad (4)$$

According to Eqs. (3) and (4), F^- is negatively charged in aqueous solution. When the pH of aqueous solution is 2, H^+ ions can protonate $–NH_2$ on the surface of PEI/DT into NH_3^+ [29]. The cationic NH_3^+ in PEI/DT can then attract and remove F^-. Adsorption occurs through the mutual attraction of positive and negative charges under electrostatic attraction. The lower the pH, the better F^- is adsorbed. The mechanistic basis of PEI/DT adsorption of fluoride ions is shown in Fig. S2. The experimental results show the highest adsorption efficiency when pH = 2.

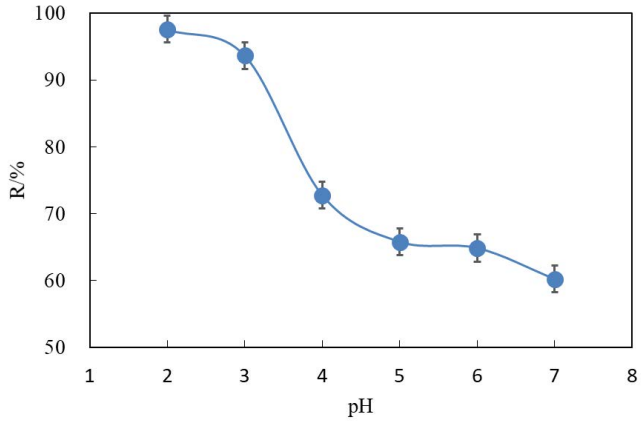

Fig. 2. Effect of different pH on adsorption of F⁻ by modified diatomite.

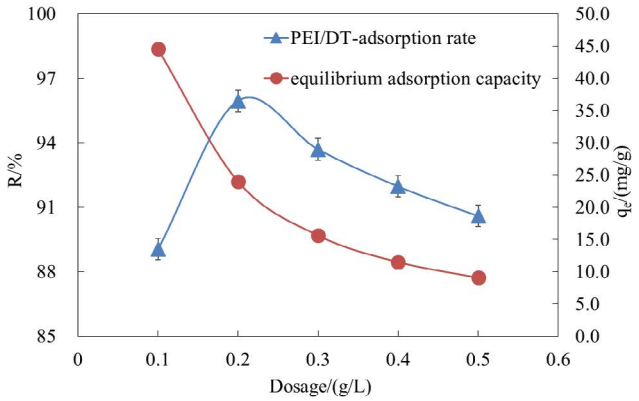

Fig. 3. Effects of different dosages on F⁻ adsorption.

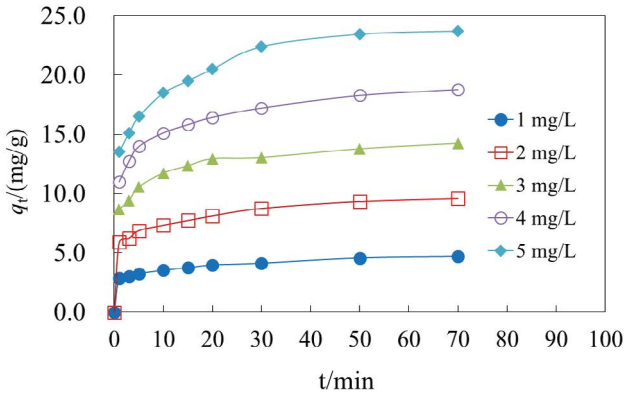

Fig. 4. Effects of contact time on F⁻ adsorption rate.

3.2.2. Effect of dosage and contact time

Fig. 3 shows the effect of PEI/DT dosage on F⁻ adsorption efficiency. The adsorption efficiency was maximum, 95.94%, at a dosage of 0.2 g/L. At higher dosage, the adsorption efficiency gradually declined, reaching 90.59% at a 0.5 g/L dosage. When the dosage increased from 0.1 to 0.2 g/L, there were more adsorption sites, so the adsorption efficiency increased significantly. However, as the dosage continued to rise, q_e fell rapidly, from 0.90 to 0.18 mg/g. This phenomenon indicates that for increased dosage of adsorbent, the adsorption capacity of the adsorbent will decrease rapidly [30]. The results show 0.2 g/L is the optimal dosage of PEI/DT for the adsorption of F⁻.

Contact time can be varied to evaluate the saturation time of adsorption process. Fig. 4 shows that the whole adsorption process reached equilibrium within 20–30 min. The adsorption efficiency increased significantly at 0–10 min and the change trend of F⁻ adsorption efficiency became stable at 10–20 min. The adsorption equilibrium time slightly differed with different initial concentration of F⁻. For an initial concentration of F⁻ of 1–3 mg/L, the equilibrium adsorption time was 20 min, but at an initial concentration of 4–5 mg/L, the equilibrium adsorption time was 30 min. The adsorption equilibrium time increased because increased F⁻ concentration resulted in longer adsorption time. In addition, equilibrium was reached quickly because adsorption occurred mainly on the surface of PEI/DT. PEI/DT has a large surface area for adsorption of F⁻, promoting combination of F⁻ with the adsorbent. With increased adsorption time, the adsorption power gradually decreased, so the adsorption efficiency slows and then finally reaches the adsorption equilibrium [31]. The results show that the optimal adsorption time is 20–30 min.

3.3. Adsorption isothermal model of fluoride ion

Adsorption isotherms show how adsorbent molecules reach equilibrium during adsorption, and the balance between adsorption time and F⁻ adsorption capacity reflects the saturated adsorption capacity of PEI/DT. Isothermal adsorption models can be used to fit the data and determine the potential mechanisms of adsorption [32]. Here, the experimental data were fit to the Langmuir and Freundlich isothermal adsorption models.

3.3.1. Langmuir adsorption isotherm

The Langmuir adsorption isotherm assumes that the adsorbent is composed of monolayers and there is no interaction between adsorbent molecules [33].

$$\frac{1}{q_e}=\frac{1}{q_e}+\frac{1}{C_e\times b\times q_m} \tag{5}$$

where C_e is the concentration of F⁻ at equilibrium, mg/L; q_m is the maximum saturated adsorption capacity, mg/g; b is a Langmuir constant, L/mg.

The fitting condition of the Langmuir model is that F⁻ concentration ranged from 1–5 mg/L at 5°C–15°C. As given in Table 1 and Fig. S3a, the results showed that the adsorption data of PEI/DT well accord with Langmuir adsorption isotherm after fitting. The q_m values of F⁻ at 5°C, 10°C and 15°C were 28.62, 23.45 and 17.39 mg/L, respectively. These results indicate that the q_m of the adsorption process decreased gradually with the increase of temperature. The adsorption capacity reached its maximum value at low

Table 1
Adsorption isothermal model parameters for F^- adsorption by PEI/DT

Pollutant	Parameters	T (°C)		
		5	10	15
Langmuir, concentration (1–5 mg/L)				
F^-	q_m (mg/g)	28.62	23.45	17.39
	b (L/mg)	9.63	12.84	18.14
	R^2	0.9960	0.9941	0.9985
Freundlich, concentration (1–5 mg/L)				
F^-	K_F (mg/g)(L/mg)$^{1/n}$	9.82	7.67	4.58
	n^{-1}	0.0075	0.3461	0.4956
	R^2	0.9613	0.9217	0.9413

Table 2
Compared the maximum saturated adsorption capacity of F^- by different adsorbents

Adsorbent	q_m (mg/g)	pH	References
Ti-zeolite	1.39	6	Ma et al. [35]
Nanoparticle resin	0.88	3–5.5	Boldaji et al. [36]
Modified bentonite	2.26	10	Thakre et al. [37]
Chitosan-Fe_3O_4 nanocomposite	2.03	3	Dehghani et al. [12]
Hydrotalcite/chitosan composite	35.20	3	Viswanathan and Meenakshi
Nano-hydroxyapatite–chitin composite	13.51	3	Sundaram and Meenakshi [39]
PEI/DT	28.62	2	This work

temperature (5°C), and the correlation coefficients (R^2) were 0.9960, 0.9941 and 0.9985 for 5°C, 10°C and 15°C, respectively. The results showed that the Langmuir isotherm is suitable to describe the adsorption of F^- on PEI/DT, suggesting that this adsorption process is a monolayer process [34].

Adsorption by this material was compared to that previously reported for different adsorbents, as shown in Table 2. The maximum saturated adsorption capacities of Ti-zeolite, nanoparticle resin, Modified bentonite, chitosan-Fe_3O_4 nanocomposite, hydrotalcite/chitosan composite, and nano-hydroxyapatite–chitin composite were determined as 1.39, 0.88, 2.26, 2.03, 35.20 and 13.51 mg/g, respectively [35–37,12,38,39]. There was low adsorption capacity of metal-supported adsorbents (Ti-zeolite, nanoparticle resin, modified bentonite, chitosan-Fe_3O_4 nanocomposite), with improved adsorption capacity of high polymer modified adsorbents (hydrotalcite/chitosan composite and nano-hydroxyapatite–chitin composite) [35–37,12,38,39]. In this work, the adsorption capacity of PEI-modified diatomite for F^- was 28.62 mg/g, higher than that reported for other adsorbents, and this modification method achieved the highest adsorption capacity at 5°C. The temperature of mine water is typically below 10°C year-round in western China, suggesting that the prepared PEI/DT is well-suited for F^- adsorption in actual mine water at low temperature.

3.3.2. Freundlich adsorption isotherm

The Freundlich model describes the adsorption of multi-molecular layers, assuming that the surface of the adsorbent is not uniform, with a change in adsorption surface energy with the change of surface coverage [40]. This model cannot calculate the saturated adsorption capacity, but is suitable for the characterization of non-uniformity monolayer adsorption and adsorption at medium concentration.

$$\ln q_e = \ln K_F + \frac{1}{n} C_e \tag{6}$$

where K_F is a Freundlich constant, (mg/g)(L/mg)$^{1/n}$; n is a Freundlich constant. If the value of $1/n$ is between 0 and 1, the material is easily adsorbed. When the value of $1/n$ is greater than 2, the material is difficult to be adsorbed.

Fig. S3b and Table 1 present the Freundlich adsorption isotherm data for PEI/DT adsorption of F^-. All the parameters in the whole adsorption process were in the range of $0 < n^{-1} < 1$, but R^2 differed greatly at different temperatures (0.9217–0.9613). This phenomenon indicates that when n^{-1} is in the range of 0–1, the surface or adsorption strength of modified diatomite is not uniform, and the material can be easily adsorbed on the surface [41]. The difference of R^2 values at different temperatures indicates that the adsorption of fluoride ions on modified diatomite at low temperature is more consistent with Langmuir adsorption isotherm model. The Freundlich model is mostly used to describe the adsorption of multi-molecular layers. Comparison of the R^2 for the two models suggests that the Langmuir model can better describe the adsorption process of PEI/DT than the Freundlich model.

3.4. Adsorption kinetics of fluoride ion adsorption

To better describe the adsorption process and explain the control principle from the perspective of dynamics, a kinetic model is needed [42]. Pseudo-first-order kinetics and pseudo-second-order kinetics were tested to describe the reaction pathways and rate control steps for adsorption of F^- by PEI/DT.

3.4.1. Pseudo-first-order kinetics model

The pseudo-first-order kinetic model was originally proposed by Lagergren and its expression is as follows [43]:

$$\log\left(q_e - q_t\right) = \log q_e - \frac{k_1 t}{2.303} \tag{7}$$

where q_e is the experimental equilibrium adsorption capacity of adsorbent, mg/g; q_t is the equilibrium adsorption capacity of adsorbent at t moment, mg/g; $q_{e,\mathrm{cal}}$ and $q_{e,\mathrm{exp}}$ are theoretical and practical equilibrium adsorption capacities, mg/g; k_1 is the pseudo-first-order kinetics model constant, 1/min.

Table 3
Kinetic model of adsorption of F^- by PEI/DT at different concentrations

Pollutant	C_0 (mg/L)	Pseudo-first-order kinetics			Pseudo-second-order kinetics			$q_{e,exp}$ (mg/g)
		$q_{e,cal}$ (mg/g)	k_1 (min^{-1})	R^2	$q_{e,cal}$ (mg/g)	k_2 (g/mg·min)	R^2	
F^-	1	7.01	0.096	0.8214	8.88	0.226	0.9991	8.91
	2	2.64	0.162	0.6615	9.58	9.136	0.9999	9.59
	3	4.03	0.053	0.6156	8.51	0.820	0.9997	8.52
	4	5.12	0.034	0.7459	9.11	0.238	0.9984	9.15
	5	6.81	0.046	0.8145	9.10	0.211	0.9987	9.06

Linear fitting of data was carried out using Eq. (7), as listed in Table 3 and Fig. S4a. The $q_{e,cal}$ value was lower than the $q_{e,exp}$ value, with a clear difference between the values. The R^2 values were 0.6156–0.8214, indicating that the adsorption experimental data do not conform to the pseudo-first-order kinetics model. These results suggest that this model cannot completely describe the adsorption process, and may only be applicable to the initial stage of adsorption [44].

3.4.2. Pseudo-second-order kinetics model

The pseudo-second-order kinetic model was proposed by Ho and Mckay [45] and can be used for in-depth analysis of dynamic data. The model is expressed as follows:

$$\frac{t}{q_t} = \frac{1}{k_2 q_e^2} + \frac{t}{q_e} \tag{8}$$

where k_2 is the pseudo-second-order kinetic model constant, g/(mg·min).

Table 3 and Fig. S4b present the linear fitting of data to the pseudo-second-order kinetic model. Compared with the pseudo-first-order kinetic model, the calculated R^2 value of the pseudo-second-order kinetic model was much closer to 1.000, with close values of $q_{e,cal}$ and $q_{e,exp}$. The overall R^2 values were between 0.9984–0.9999, indicating that the pseudo-second-order kinetic model is more suitable to describe the experimental data of F^- adsorption by PEI/DT. The experimental results indicated that chemical adsorption may be the limiting step affecting the adsorption efficiency of PEI/DT [46]. Amino groups on the surface play a key role in the interaction between F^- and PEI/DT, and the F^- is mainly adsorbed on the surface of PEI/DT.

3.5. Adsorption thermodynamics

Thermodynamic parameters, including Gibbs free energy ($\Delta G°$), enthalpy change ($\Delta H°$), and entropy change ($\Delta S°$), are important indexes for the application of adsorption process and were determined according to the following equations.

$$\Delta G° = -RTK_d \tag{9}$$

$$\ln K_d = \frac{\Delta S°}{R} - \frac{\Delta H°}{RT} \tag{10}$$

Table 4
Thermodynamic parameters for adsorption of fluoride ion by PEI/DT

Pollutant	C_0	$\Delta G°$ (kJ/mol)			$\Delta H°$	$\Delta S°$
	(mg/L)	278 K	283 K	288 K	(kJ/mol)	(J/mol·K)
F^-	1	–7.41	–6.88	–5.45	–24.97	–11.80
	2	–8.24	–4.45	–5.92	–30.81	–21.71
	3	–8.91	–5.41	–5.43	–29.75	–26.97
	4	–6.51	–6.51	–4.32	–20.91	–21.11
	5	–4.41	–4.72	–5.14	–31.14	–82.41

$$K_d = \frac{q_e}{C_e} \tag{11}$$

$$\Delta G° = \Delta H° - T\Delta S° \tag{12}$$

where R is the gas constant (8.314 J/mol·K), T is the temperature (K), and K_d is the partition coefficient. K_d was calculated from Eq. (11), $\Delta H°$ and $\Delta S°$ were calculated from Eqs. (10) and (12), respectively.

The data calculated according to Eqs. (9)–(12) are listed in Table 4. As shown, all the values of $\Delta G°$ and $\Delta H°$ obtained at different temperatures are negative, indicating that adsorption is a spontaneous exothermic process. As the temperature increased, q_e gradually decreased. $\Delta S°$ value is a physical quantity reflecting the disorder degree of material. When $\Delta S°$ is positive, it indicates an increased disorder degree in solid–liquid phase. A negative value indicates that $\Delta H°$ plays a leading role in spontaneous adsorption ($\Delta G° < 0$) [47]. Overall, the results show that the adsorption of fluoride ions by the prepared material is a spontaneous exothermic process.

4. Conclusion

In this work, we used polyethylenimine modified diatomite to adsorb low concentration F^- (1–5 mg/L) in aqueous solution. FTIR analysis confirmed that the amino functional groups (–NH_2) were successfully loaded onto the surface of diatomite. The optimal values of pH, dosage, and contact time were determined to be 2.0, 0.2 g/L, and 30 min, respectively. The adsorption process achieved the best adsorption efficiency (97.56%) at 5°C, indicating

that this material is appropriate for use in low temperature mine water. The isothermal adsorption model confirmed that the adsorption process well fit to the Langmuir model, with a maximum saturated adsorption capacity of 28.62 mg/g. The pseudo-second-order kinetic model better described the adsorption process than the pseudo-first-order kinetic model, with average R^2 value of 0.9992. Finally, the thermodynamic parameters confirm that the adsorption of F^- by PEI/DT is a spontaneous exothermic process. This work provides a new idea for the application of PEI/DT as an efficient F^- adsorbent.

Acknowledgement

This work was supported by the Open Fund of the State Key Laboratory of Water Resource Protection and Utilization in Coal Mining (Grant No. GJNY-18-73.14), the National Natural Science Foundation of China (Grants No. 52000060), and the Henan provincial key science and technology research project (222102110136).

References

[1] M. Ren, L. Zheng, D. Wang, X. Chen, X. Dong, X. Wei, H. Cheng, Copper isotope ratios allowed for quantifying the contribution of coal mining and combustion to total soil copper concentrations in China, Environ. Pollut., 308 (2022) 119613, doi: 10.1016/j.envpol.2022.119613.

[2] Y. Huang, J. Wang, J. Li, M. Lu, Y. Guo, L. Wu, Q. Wang, Ecological and environmental damage assessment of water resources protection mining in the mining area of Western China, Ecol. Indic., 139 (2022) 108938, doi: 10.1016/j.ecolind.2022.108938.

[3] C.J. Chuah, H.R. Lye, A.D. Ziegler, S.H. Wood, C. Kongpun, S. Rajchagool, Fluoride: a naturally-occurring health hazard in drinking-water resources of Northern Thailand, Sci. Total Environ., 545 (2016) 266–279.

[4] J. He, Y. Yang, Z. Wu, C. Xie, K. Zhang, L. Kong, J. Liu, Review of fluoride removal from water environment by adsorption, J. Environ. Chem. Eng., 8 (2020) 104516, doi: 10.1016/j.jece.2020.104516.

[5] Y.S. Solanki, M. Agarwal, A.B. Gupta, S. Gupta, P. Shukla, Fluoride occurrences, health problems, detection, and remediation methods for drinking water: a comprehensive review, Sci. Total Environ., 807 (2022) 150601, doi: 10.1016/j.scitotenv.2021.150601.

[6] Y. Zhang, S. Liang, R. He, J. Zhao, J. Lv, W. Kang, J. Zhang, Enhanced adsorption and degradation of antibiotics by doping corncob biochar/PMS with heteroatoms at different preparation temperatures: mechanism, pathway, and relative contribution of reactive oxygen species, J. Water Process Eng., 46 (2022) 102626, doi: 10.1016/j.jwpe.2022.102626.

[7] Y. Zhang, M. Yin, X. Sun, J. Zhao, Implication for adsorption and degradation of dyes by humic acid: light driven of environmentally persistent free radicals to activate reactive oxygen species, Bioresour. Technol., 307 (2020) 123183, doi: 10.1016/j.biortech.2020.123183.

[8] A. Ezzeddine, A. Bedoui, A. Hannachi, N. Bensalah, Removal of fluoride from aluminum fluoride manufacturing wastewater by precipitation and adsorption processes, Desal. Water Treat., 54 (2015) 2280–2292.

[9] Y. Zhang, H. Wan, J. Zhao, J. Li, Biosorption of anionic and cationic dyes *via* raw and chitosan oligosaccharide-modified Huai Flos Chrysanthemum at different temperatures, RSC Adv., 9 (2019) 11202–11211.

[10] C.F.Z. Lacson, M.C. Lu, Y.H. Huang, Fluoride-containing water: a global perspective and a pursuit to sustainable water defluoridation management-an overview, J. Cleaner Prod., 280 (2021) 124236, doi: 10.1016/j.jclepro.2020.124236.

[11] Z. Wang, J. Su, X. Hu, A. Ali, Z. Wu, Isolation of biosynthetic crystals by microbially induced calcium carbonate precipitation and their utilization for fluoride removal from groundwater, J. Hazard. Mater., 406 (2021) 124748, doi: 10.1016/j.jhazmat.2020.124748.

[12] M.H. Dehghani, R.R. Karri, E.C. Lima, A.H. Mahvi, S. Nazmara, A.M. Ghaedi, M. Fazlzadeh, S. Gholami, Regression and mathematical modeling of fluoride ion adsorption from contaminated water using a magnetic versatile biomaterial & chelating agent: insight on production & experimental approaches, mechanism and effects of potential interferers, J. Mol. Liq., 315 (2020) 113653, doi: 10.1016/j.molliq.2020.113653.

[13] J. Cheng, X. Meng, C. Jing, J. Hao, La^{3+}-modified activated alumina for fluoride removal from water, J. Hazard. Mater., 278 (2014) 343–349.

[14] Z. Zhao, C. Geng, C. Yang, F. Cui, Z. Liang, A novel flake-ball-like magnetic Fe_3O_4/γ-MnO_2 meso-porous nanocomposite: adsorption of fluorinion and effect of water chemistry, Chemosphere, 209 (2018) 173–181.

[15] X. Ren, Q. Wang, X. Chen, Y. He, R. Li, J. Li, Z. Zhang, Pathways and mechanisms of nitrogen transformation during co-composting of pig manure and diatomite, Bioresour. Technol., 329 (2021) 124914, doi: 10.1016/j.biortech.2021.124914.

[16] B. Wang, M. Xiong, B. Shi, Z. Li, H. Zhang, Treatment of shale gas flowback water by adsorption on carbon-nanotube-nested diatomite adsorbent, J. Water Process Eng., 42 (2021) 102074, doi: 10.1016/j.jwpe.2021.102074.

[17] J. Xiang, H. Li, Y. Hei, G. Tian, L. Zhang, P. Cheng, J. Zhang, N. Tang, Preparation of highly permeable electropositive nanofiltration membranes using quaternized polyethylenimine for dye wastewater treatment, J. Water Process Eng., 48 (2022) 102831, doi: 10.1016/j.jwpe.2022.102831.

[18] E. Altıntıg, H. Altundag, M. Tuzen, A. Sarı, Effective removal of methylene blue from aqueous solutions using magnetic loaded activated carbon as novel adsorbent, Chem. Eng. Res. Des., 122 (2017) 151–163.

[19] M. Tuzen, A. Sarı, T.A. Saleh, Response surface optimization, kinetic and thermodynamic studies for effective removal of rhodamine B by magnetic AC/CeO_2 nanocomposite, J. Environ. Manage., 206 (2018) 170–177.

[20] E. Altıntıg, M. Yenigun, A. Sarı, H. Altundag, M. Tuzen, T.A. Saleh, Facile synthesis of zinc oxide nanoparticles loaded activated carbon as an eco-friendly adsorbent for ultra-removal of malachite green from water, Environ. Technol. Innovation, 21 (2021) 101305, doi: 10.1016/j.eti.2020.101305.

[21] Y. Zhang, M. Xu, S. Liang, Z. Feng, J. Zhao, Mechanism of persulfate activation by biochar for the catalytic degradation of antibiotics: synergistic effects of environmentally persistent free radicals and the defective structure of biochar, Sci. Total Environ., 794 (2021) 148707, doi: 10.1016/j.scitotenv.2021.148707.

[22] Y. Zhang, M. Xu, X. Liu, M. Wang, J. Zhao, S. Li, M. Yin, Regulation of biochar mediated catalytic degradation of quinolone antibiotics: important role of environmentally persistent free radicals, Bioresour. Technol., 326 (2021) 124780, doi: 10.1016/j.biortech.2021.124780.

[23] Y. Zhang, X. Sun, W. Bian, J. Peng, H. Wan, J. Zhao, The key role of persistent free radicals on the surface of hydrochar and pyrocarbon in the removal of heavy metal-organic combined pollutants, Bioresour. Technol., 318 (2020) 124046, doi: 10.1016/j.biortech.2020.124046.

[24] B. Galzerano, P. Aprea, L. Verdolotti, M.S. de Luna, C. Ascione, D. Caputo, M. Lavorgna, E. Migliore, B. Liguori, Effect of carbonaceous fillers on adsorption behavior of multifunctional diatomite-based foams for wastewater treatment, Chemosphere, 281 (2021) 130999, doi: 10.1016/j.chemosphere.2021.130999.

[25] Y. Fang, M. Wu, Q. Zhang, F. Zhou, C. Deng, Y. Yan, H. Shen, Y. Tang, Y. Wang, Hierarchical covalent organic frameworks-modified diatomite for efficient separation of bisphenol A from water in a convenient column mode, Sep. Purif. Technol., 298 (2022) 121611, doi: 10.1016/j.seppur.2022.121611.

[26] A. Hethnawi, W. Khderat, K. Hashlamoun, A. Kanan, N.N. Nassar, Enhancing chromium(VI) removal from synthetic and real tannery effluents by using diatomite-embedded

nanopyroxene, Chemosphere, 252 (2020) 126523, doi: 10.1016/j.chemosphere.2020.126523.
[27] A. Hethnawi, N.N. Nassar, A.D. Manasrah, G. Vitale, Polyethylenimine-functionalized pyroxene nanoparticles embedded on diatomite for adsorptive removal of dye from textile wastewater in a fixed-bed column, Chem. Eng. J., 320 (2017) 389–404.
[28] P. Zhang, Y. Cui, K. Zhang, S. Wu, D. Chen, Y. Gao, Enhanced thermal storage capacity of paraffin/diatomite composite using oleophobic modification, J. Cleaner Prod., 279 (2021) 123211, doi: 10.1016/j.jclepro.2020.123211.
[29] X. Zhao, Y. Che, Y. Mo, W. Huang, C. Wang, Fabrication of PEI modified GO/MXene composite membrane and its application in removing metal cations from water, J. Membr. Sci., 640 (2021) 119847, doi: 10.1016/j.memsci.2021.119847.
[30] R. Zhang, A. Ali, J. Su, J. Liu, Z. Wang, J. Li, Y. Liu, Synergistic removal of fluoride, calcium, and nitrate in a biofilm reactor based on anaerobic microbially induced calcium precipitation, J. Hazard. Mater., 428 (2022) 128102, doi: 10.1016/j.jhazmat.2021.128102.
[31] F.A. Udenby, H. Almuhtaram, M.J. McKie, R.C. Andrews, Adsorption of fluoranthene and phenanthrene by virgin and weathered polyethylene microplastics in freshwaters, Chemosphere, 307 (2022) 135585, doi: 10.1016/j.chemosphere.2022.135585.
[32] X. Chen, M.F. Hossain, C. Duan, J. Lu, Y.F. Tsang, M.S. Islam, Y. Zhou, Isotherm models for adsorption of heavy metals from water-a review, Chemosphere, 307 (2022) 135545, doi: 10.1016/j.chemosphere.2022.135545.
[33] X. Zhang, N. Yuan, S. Xu, Y. Li, Q. Wang, Efficient adsorptive elimination of organic pollutants from aqueous solutions on ZIF-8/MWCNTs-COOH nanoadsorbents: adsorption kinetics, isotherms, and thermodynamic study, J. Ind. Eng. Chem., 111 (2022) 155–167.
[34] B. Noroozi, G.A. Sorial, Applicable models for multi-component adsorption of dyes: a review, J. Environ. Sci., 25 (2013) 419–429.
[35] Z. Ma, Q. Zhang, X. Weng, C. Mang, L. Si, Z. Guan, L. Cheng, Fluoride ion adsorption from wastewater using magnesium(II), aluminum(III) and titanium(IV) modified natural zeolite: kinetics, thermodynamics, and mechanistic aspects of adsorption, J. Water Reuse Desal., 8 (2018) 479–489.
[36] M.R. Boldaji, R. Nabizadeh, M.H. Dehghani, K. Nadafi, A.H. Mahvi, Evaluating the performance of iron nanoparticle resin in removing arsenate from water, J. Environ. Sci. Health., Part A, 45 (2010) 946–950.
[37] D. Thakre, S. Rayalu, R. Kawade, S. Meshram, J. Subrt, N. Labhsetwar, Magnesium incorporated bentonite clay for defluoridation of drinking water, J. Hazard. Mater., 180 (2010) 122–130.
[38] N. Viswanathan, S. Meenakshi, Selective fluoride adsorption by a hydrotalcite/chitosan composite, Appl. Clay Sci., 48 (2010) 607–611.
[39] C.S. Sundaram, S. Meenakshi, Fluoride sorption using organic–inorganic hybrid type ion exchangers, J. Colloid Interface Sci., 333 (2009) 58–62.
[40] S. Sharma, G. Sharma, A. Kumar, T.S. AlGarni, M. Naushad, Z.A. ALOthman, F.J. Stadler, Adsorption of cationic dyes onto carrageenan and itaconic acid-based superabsorbent hydrogel: synthesis, characterization and isotherm analysis, J. Hazard. Mater., 421 (2022) 126729, doi: 10.1016/j.jhazmat.2021.126729.
[41] X. Ma, Y. Liu, Q. Zhang, S. Sun, X. Zhou, Y. Xu, A novel natural lignocellulosic biosorbent of sunflower stem-pith for textile cationic dyes adsorption, J. Cleaner Prod., 331 (2022) 129878, doi: 10.1016/j.jclepro.2021.129878.
[42] H. Wang, Z. Li, S. Yahyaoui, H. Hanafy, M.K. Seliem, A. Bonilla-Petriciolet, D.G. Luiz, L. Sellaoui, Q. Li, Effective adsorption of dyes on an activated carbon prepared from carboxymethyl cellulose: experiments, characterization and advanced modelling, Chem. Eng. J., 417 (2021) 128116, doi: 10.1016/j.cej.2020.128116.
[43] H. Yuh-Shan, Citation review of Lagergren kinetic rate equation on adsorption reactions, Scientometrics, 59 (2004) 171–177.
[44] X. Liang, J. Zhang, M. Li, K. Wang, G. Luo, Dynamic interfacial tension and adsorption kinetics of nonionic surfactants during microfluidic droplet formation process, Chem. Eng. J., 445 (2022) 136658, doi: 10.1016/j.cej.2022.136658.
[45] R. Wagner, S. Bag, T. Trunzer, G.P. Fraga, W. Wenzel, S. Berensmeier, M. Franzerb, Adsorption of organic molecules on carbon surfaces: experimental data and molecular dynamics simulation considering multiple protonation states, J. Colloid Interface Sci., 589 (2021) 424–437.
[46] M. Loganathan, A.S. Raj, A. Murugesan, P.S. Kumar, Effective adsorption of crystal violet onto aromatic polyimides: kinetics and isotherm studies, Chemosphere, 304 (2022) 135332, doi: 10.1016/j.chemosphere.2022.135332.
[47] H.N. Tran, E.C. Lima, R.S. Juang, J.C. Bollinger, H.P. Chao, Thermodynamic parameters of liquid-phase adsorption process calculated from different equilibrium constants related to adsorption isotherms: a comparison study, J. Environ. Chem. Eng., 9 (2021) 106674, doi: 10.1016/j.jece.2021.106674.

Supplementary information:

Table S1
Element content in diatomite

Elements	SiO_2	Al_2O_3	Fe_2O_3	CaO	MgO	K_2O	Others
Contents	75.43%	5.87%	1.51%	5.75%	3.02%	2.34%	6.08%

Table S2
Analysis of specific surface area and pore structure of adsorbent

Names	Specific surface area (m^2/g)	Total pores (cm^3)	Average pores (nm)
Diatomite	65.86	0.0556	3.38
PEI/DT	47.07	0.0331	4.89

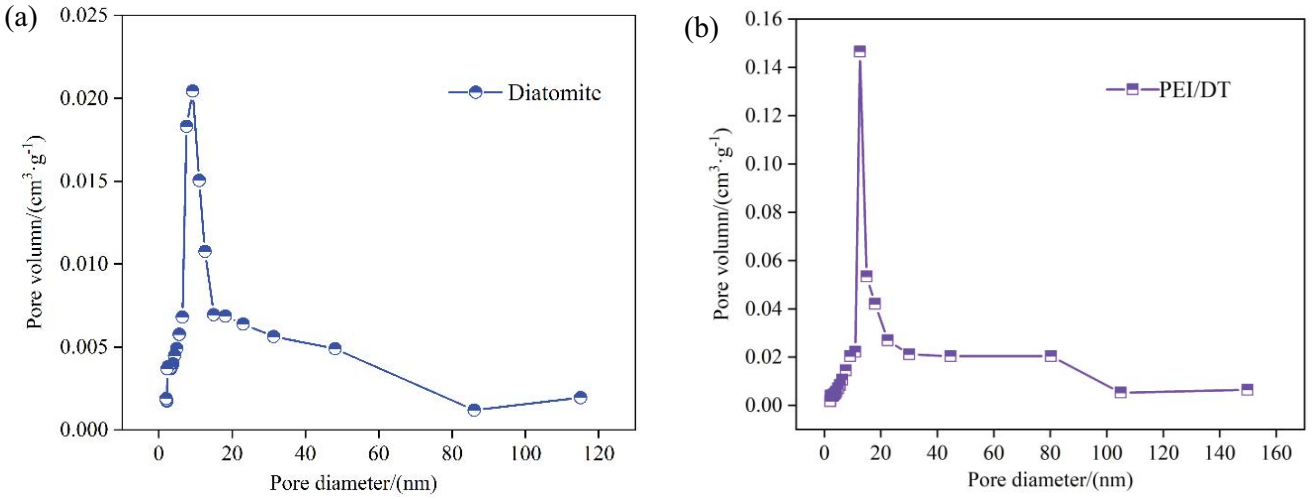

Fig. S1. Pore-size distribution of PEI/DT and diatomite.

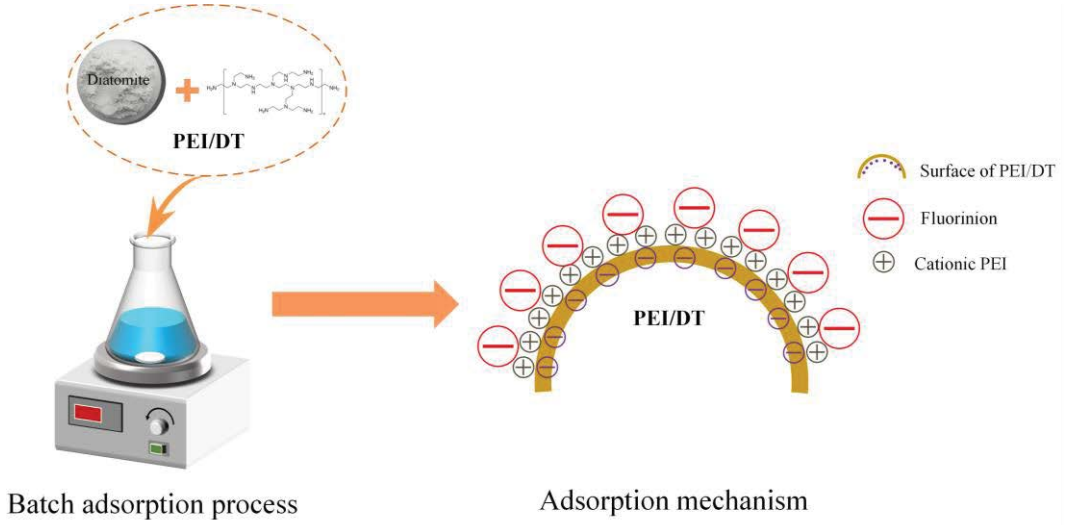

Fig. S2. Batch adsorption process and mechanism.

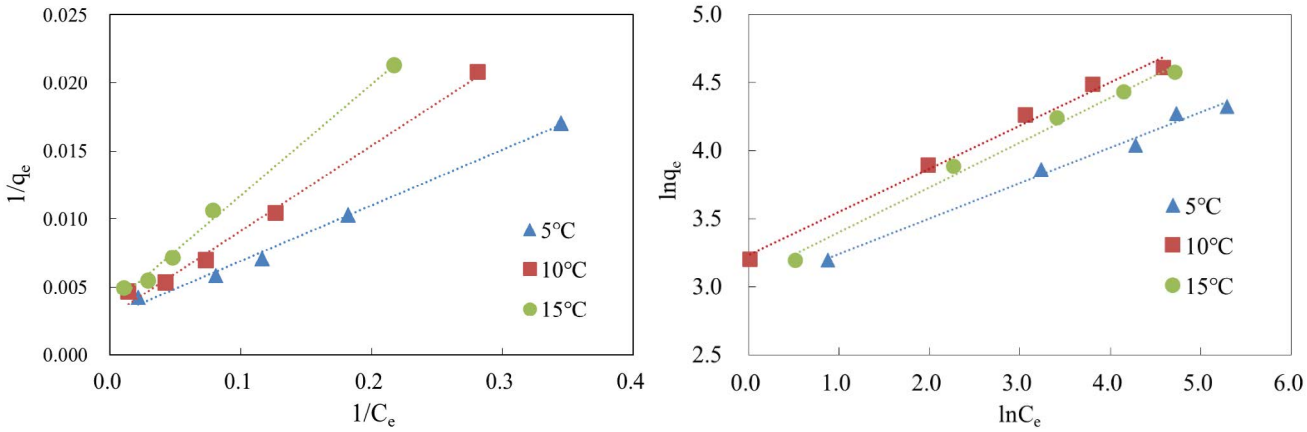

(a) Langmuir b) Freundlich

Fig. S3. Fitting data graph of the isothermal adsorption models: (a) Langmuir and (b) Freundlich.

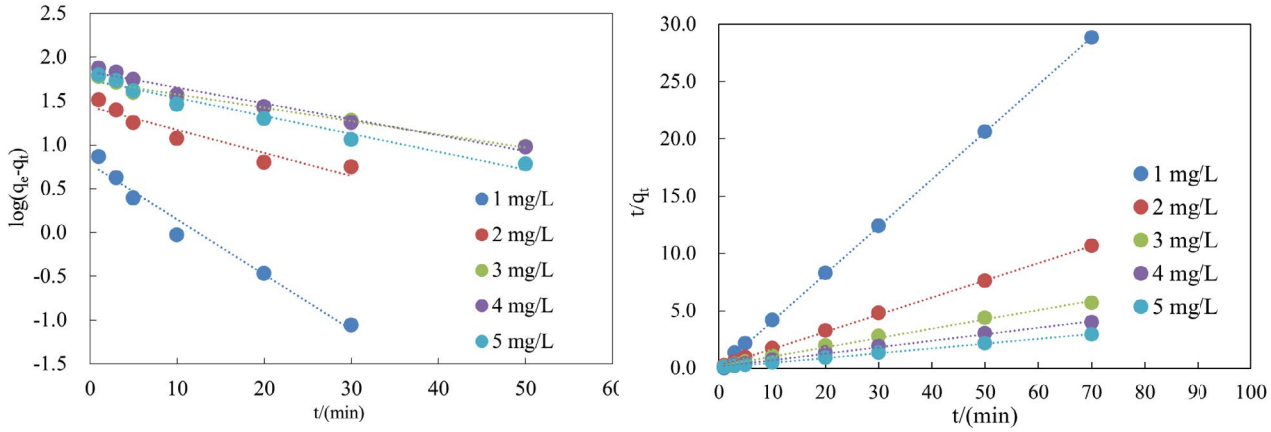

(a) Pseudo-first-order kinetic model (b) pseudo-second-order model

Fig. S4. Kinetic models for adsorption of F^- by PEI/DT: (a) pseudo-first-order kinetic model and (b) pseudo-second-order model.